THE JOURNAL OF BIOLOGICAL CHEMISTRY Vol. 273, No. 26, Issue of June 26, pp. 16248–16258, 1998
Printed in U.S.A.

Conformational Changes in Conantokin-G Induced upon Binding of Calcium and Magnesium as Revealed by NMR Structural Analysis*

(Received for publication, December 19, 1997, and in revised form, April 1, 1998)

Zhigang Chen‡, Tamas Blandl§, Mary Prorok§, Scott E. Warder§, Leping Li¶, Yi Zhu‡, Lee G. Pedersen¶‖, Feng Ni‡, and Francis J. Castellino§**

From the §Department of Chemistry and Biochemistry, University of Notre Dame, Notre Dame, Indiana 46556, the ‡Biomolecular NMR Laboratory and the Montreal Joint Center for Structural Biology, Biotechnology Research Institute, National Research Council of Canada, Montreal, Quebec H4P 2R2, Canada, ¶NIEHS, Research Triangle Park, North Carolina 27709, and the ‖Department of Chemistry, University of North Carolina, Chapel Hill, North Carolina 27599

The apo- and metal-bound solution conformations of synthetic conantokin-G (con-G, $G^1E\gamma\gamma L^5Q\gamma NQ\gamma^{10}$-$LIR\gamma K^{15}SN$-$CONH_2$, γ = γ-carboxyglutamic acid), an antagonist of *N*-methyl-D-aspartate receptor-derived neuronal ion channels, have been examined by one- and two-dimensional ^1H NMR at neutral pH. A complete structure for the Mg^{2+}-loaded peptide was defined by use of distance geometry calculations and was found to exist as an α-helix that spans the entire peptide. The α-helical nature of Mg^{2+}/con-G was also supported by the small values (<5.5 Hz) of the $^3J_{HN\alpha}$ coupling constants measured for amino acid residues 3–5, 8, 9, and 11–16, and the small values (<4 ppb/K) of the temperature coefficients observed for the αNH protons of residues 5–17. This conformation contrasted with that obtained for apo-con-G, which was nearly structureless in solution. Docking of Mg^{2+} into con-G was accomplished by use of the genetic algorithm/molecular dynamics simulation method, employing the NMR-derived Mg^{2+}-loaded structure for initial coordinates in the midpoint calculations. For the 3 Mg^{2+}/con-G model, it was found that binding of one Mg^{2+} ion is stabilized by oxygen atoms from three γ-carboxylates of Gla^3, Gla^4, and Gla^7; another Mg^{2+} is coordinated by two oxygen atoms, one from each of the γ-carboxylates of Gla^7; and a third metal ion through three donor oxygen atoms of γ-carboxylates from Gla^{10} and Gla^{14}. As shown from direct metal binding measurements to mutant con-G peptides, these latter two Gla residues probably stabilized the tightest binding Mg^{2+} ion. Circular dichroism studies of these same peptide variants demonstrated that all Gla residues contribute to the adoption of the Mg^{2+}-dependent α-helical conformation in con-G.

The data obtained in this investigation provide a molecular basis for the large conformational alteration observed in apo-con-G as a result of divalent cation binding and allow assessment of the roles of individual Gla residues in defining certain of the structure-function properties of con-G.

Conotoxins are small peptides present in the venoms of predator snails of the genus *Conus*. These pharmacologically active materials are employed by the snails to paralyze their prey by envenomation, thus enhancing their effectiveness as predators of fish, mollusks, and polychaete worms (reviewed in Ref. 1). A large number of these types of peptides are used by a variety of species of these snails. Consequently, the structures and functions of the peptides are diverse. The conotoxins are broadly divided into three classes, those that function via effects on acetylcholine receptors (α-conotoxins), muscle Na^+ channels (μ-conotoxins), or voltage-sensitive Ca^{2+}-channels (ω-conotoxins). In general, these small peptides are highly conformationally constrained, in part due to disulfide bridges, *viz.*, 2–4 disulfide loops over peptide stretches of 10–30 amino acids. These types of constraints likely provide a smaller distribution of possible conformations for these peptides, which in turn might govern their tight receptor binding properties. Because of their high functional selectivity, many different *Conus* peptides are employed as probes of specific receptors (2).

Two *Conus*-derived venomous peptides of the conantokin class have been well characterized. Referred to as con-G[1] (3) and con-T (4), they contain 17 and 21 amino acid residues, respectively. These neuroactive peptides target for their functions the ligand-gated Ca^{2+}/Na^+ channels of the NMDA-R subtype, acting as noncompetitive inhibitors of ion flow through the channels. On a molecular level, this property is based on the noncompetitive inhibition by the conantokins of the positive allosteric effects of polyamines on this receptor (5). Structurally, the conantokins lack disulfide bonds. However, these peptides contain a very high relative amount of Gla, specifically, 5 mol/mol in con-G and 4 mol/mol in con-T. Because of this feature, it is likely that some of the conformational stability that is lacking due to the absence of disulfide bonds might be accommodated by the divalent cation binding afforded these peptides by the presence of Gla residues. This metal ion binding, the thermodynamic characteristics of which have been described, might enhance the receptor binding properties of these peptides by reducing the range of their possible conformations (6). Therefore, recent activity in several laboratories has centered on structures of the apo- and cation-loaded forms of these peptides.

We have shown from CD measurements that apo-con-G is relatively structureless, but its conformation is nearly entirely

* This work was supported by Grants HL-19982 (to F. J. C.) and HL-27995 (to L. G. P.) from the National Institutes of Health, the Kleiderer-Pezold family endowed professorship (to F. J. C.), Grant MT-12566 from the Medical Research Council of Canada (to F. N.), the National Research Council of Canada (NRCC Publication No. 41411), a grant from Ciba-Geigy Canada Ltd. (to F. N.), and predoctoral (to S. E. W.) and postdoctoral (to M. P.) fellowships from the American Heart Association, Indiana Affiliate. The costs of publication of this article were defrayed in part by the payment of page charges. This article must therefore be hereby marked "*advertisement*" in accordance with 18 U.S.C. Section 1734 solely to indicate this fact.

** To whom correspondence should be addressed. Tel.: 219-631-6456; Fax: 219-631-8149; E-mail: castellino.1@nd.edu.

[1] The abbreviations used are: ACh, acetylcholine; con-G, conantokin-G; con-T, conantokin-T; Gla, γ-carboxyglutamic acid; NMDA-R, *N*-methyl-D-aspartate receptor; PAL, 5-(4-(9-fluorenylmethyloxycarbonyl)-aminomethyl-3,5-dimethoxy-phenoxy) valeric acid; Fmoc, 9-fluorenylmethyloxycarbonyl; *O*-tBu, *t*-butyl ester; CD, circular dichroism; ITC, isothermal calorimetry; NOE, nuclear Overhauser effect; Mes, 4-morpholineethanesulfonic acid.

α-helical when the peptide is saturated with Ca^{2+} and Mg^{2+}. On the other hand, con-T contains a high relative amount of α-helix in both states (6). This former conclusion is in basic agreement with studies employing Fourier transformed-infrared spectroscopy (2), but it is at variance with NMR studies that were designed to probe these same structures (7) and with a study based on CD measurements (8), in which it was concluded that significant amounts of helical conformations were present in the metal-free form of con-G. Because of the possible importance of the metal ion-induced conformational alteration of con-G, we undertook a solution structural analysis of con-G in its metal-free and Ca^{2+}- and Mg^{2+}-loaded forms, using one- and two-dimensional ^1H NMR. Although other NMR studies have been published for the apo- and Ca^{2+}-dependent forms of con-G (7, 9), as well as apo-con-T (9, 10), they have mainly focused on backbone conformations. We recently performed extensive ^1H NMR studies on the solution conformation of apo-con-T (11) and Ca^{2+}/con-T (12), allowing establishment of both backbone and side-chain conformations. This same strategy has now been applied to con-G to determine the backbone and side-chain conformations of the metal-bound form. Results of this structural analysis, as well as direct metal binding and CD measurements of wild-type and mutant Con-G peptides, are presented in the current report.

EXPERIMENTAL PROCEDURES

Peptide Synthesis—Con-G ($G^1E\gamma\gamma L^5Q\gamma NQ\gamma^{10}LIR\gamma K^{15}SN$-$CONH_2$) was synthesized by Fmoc chemistry on an Applied Biosystems (Foster City, CA) model 433A peptide synthesizer using 5-(4-(9-fluorenylmethyloxycarbonyl)-aminomethyl-3,5-dimethoxy-phenoxy) valeric acid resin (PerSeptive Biosystems, Framingham, MA). The N^{α}-Fmoc-(γ,γ'-di-*O*-tBu)-L-Gla and N^{α}-Fmoc-(γ,γ'-di-*O*-tBu)-D-Gla employed were chemically synthesized, as described previously (13). All other N^{α}-Fmoc-L-amino acids used in the synthesis of con-G were purchased from Sigma or Nova Biochem (La Jolla, CA). The following side-chain protecting groups were present on the amino acids: Arg(N^G-2,2,5,7,8-pentamethylchroman-6-sulfonyl), Asn(N^{γ}-trityl), Gln(N^{δ}-trityl), Glu(*O*-tBu), Lys(N^{ϵ}-*t*-butyloxycarbonyl), and Ser(*O*-tBu). The protocols employed for synthesis, deprotection, and purification of the resulting con-G have been described earlier (6). After deblocking, the peptide contained an amidated carboxyl terminus, as is the case for naturally occurring con-G.

Sample Preparation—The samples for NMR measurements were prepared by dissolving appropriate amounts of the purified peptide in 450 μl of a buffered solution containing 10 mM $NaBO_3$, 100 mM NaCl, pH 6.5. A volume of 50 μl of ^2H_2O was added to the peptide solutions to provide the ^2H lock signal. 4,4-Dimethyl-4-silapentane-1-sulfonate was added as an internal reference. Peptide concentrations were approximately 1 mM for one-dimensional and 2 mM for two-dimensional NMR experiments. Stock solutions of $CaCl_2$ and $MgCl_2$ at concentrations of 0.2 M were prepared in the same buffer used for the peptide samples. In some experiments, $CaCl_2$ and $MgCl_2$ were titrated to the NMR samples of the con-G peptide at concentrations up to 20-fold in excess of that of the peptide.

NMR Measurements—All NMR experiments were carried out on a Bruker AMX2–500 MHz and/or a DRX-500 MHz spectrometer at temperatures of 5, 15, or 25 °C. The solvent H_2O signal was suppressed by use of the WATERGATE method for one-dimensional and most of the two-dimensional NMR experiments, implemented through the 3-9-19 pulse train for selective inversion (14). The two-dimensional NMR experiments included NOESY with water flip-back (15) and TOCSY (16, 17) using the TOWNY-16 spin-lock sequence (18). Water suppression in the DQF-COSY (19) experiments was achieved by presaturation during the preacquisition delay.

Two-dimensional NMR experiments were acquired using time proportional phase incrementation along the t_1 dimension for phase-sensitive detection, with a relaxation delay of 1.5–2 s (20). Mixing times of 30–60 ms were used for the TOCSY experiments, and 150 ms and 250 ms for the NOESY spectra. Free induction decays were acquired with 2K complex data points for the TOCSY and NOESY data sets and with 4K complex data points for DQF-COSY experiments. A total of 400 t_1 increments were collected for NOESY, 300–350 for TOCSY, and 512 for DQF-COSY data sets. Sine modulation was used along the t_1 dimension, with the initial t_1 delays adjusted so that the zero and first-order phase corrections along F1 were 90° and 0°, respectively (21).

The NMR data were processed using an in-house program, nmrDSP, incorporating fast cosine and sine transformation, linear prediction, and optimized baseline correction procedures. The free induction decay matrices were multiplied by cosine-squared window functions in both dimensions prior to Fourier transformation. The experimental data were extended along the t_1 dimension of the NOESY and TOCSY data sets by linear prediction to 512 points and then zero-filled to 1024 before the application of the window functions and sine transformation. The matrices of the DQF-COSY spectra were 1K × 1K real points for use in resonance assignments and were expanded to 8K (F2) × 1K (F1) for the determination of coupling constants. The DQF-COSY spectra were phased along the F2 dimension in both absorptive and dispersive modes. The splittings of cross-peak extrema were measured in both modes and were used to calculate the $^3J_{HN\alpha}$ coupling constants corrected for line width effects (22).

Proton Resonance Assignments—Residue-specific assignments of the proton resonances were achieved by spin system identification using DQF-COSY and TOCSY, followed by sequential assignments through NOE connectivities (23). Despite a number of residues with similar spin types, the dispersion of the amide proton resonances was sufficiently large to allow the complete assignments of the proton resonances in the absence and presence of metal ions. Gla residues were easily identified in a TOCSY spectrum because their γCH proton resonances appear at a lower frequency (≈3 ppm). The side-chain amide protons of Asn and Gln residues were assigned on the basis of the cross peaks in the amide region of the TOCSY spectra and intraresidue NOESY cross peaks to their βCH_2 protons. The ϵNH proton of Arg^{13} of con-G is well shifted downfield in the presence of metal ions, and its assignment was based on a strong TOCSY (and COSY) correlation to the δCH_2 protons of Arg. The guanidino protons of Arg^{13} in apo-con-G are very broad as a result of solvent exchange and appear upfield of the backbone and side-chain NH resonance envelope. In the presence of metal ions, these protons also had intraresidue NOE connectivities to the ϵNH and δCH_2 protons of Arg^{13}.

Structure Calculations—The intensities of the cross peaks in the NOESY spectra of con-G were classified from the number of contours as strong, medium, or weak and converted to distance upper bounds of 2.7, 3.7, and 5.0 Å, respectively. All side-chain/side-chain or side-chain/main-chain medium-range (i, $i + 2$ and i, $i + 4$) constraints were set to an upper bound of 5 Å and a lower bound of 2.0 Å. Starting structures were generated by distance geometry using uniquely assigned NOE constraints and with fixed bond lengths and bond angles provided in the ECEPP/3 data base (24). Averaged distances between groups of protons with resonance overlaps were required to satisfy both the upper and lower bounds of the penalty function (25, 26). These initial structures yielded information for assignment to specific proton pairs of some overlapped NOEs. Optimization of the structures was carried out by varying all dihedral angles except for the ω angles governing the planarity of the peptide bond (25–27). A set of low-energy structures was selected for further calculations incorporating all NOE distance constraints in the distance geometry minimization. Visualization of the structures was performed using the Sybyl software package (Tripos, Inc.).

Docking of Mg^{2+} in Con-G—Placement of the metal ions in con-G and further energy minimization-based refinement of the metal-bound structure were accomplished by the genetic algorithm-molecular dynamics simulation approach described previously (28). Briefly, the initial coordinates for Mg^{2+}/con-G used in the genetic algorithm midpoint calculations were those determined by NMR in this study for the Mg^{2+}/con-G complex. The initial positions of the Mg^{2+} ions were determined by searching through the O–O midpoints that were within 6 Å of each other, using all oxygen atoms in the midpoint calculation. A total of 195 midpoints were found. The lowest Amber (29) energy structure, verified also by a systematic search, was subjected to a Particle Mesh Ewald molecular dynamics simulation (30). In this case, the peptide was solvated in a 9.0-Å box, and H_2O, Na^+, and Mg^{2+} were energy-minimized at constant volume. A Particle Mesh Ewald molecular dynamics simulation was then performed on Na^+, Mg^{2+}, and H_2O for 100 ps, followed by energy minimization. The side-chain residues, the ions, and H_2O were then subjected to another Particle Mesh Ewald molecular dynamics simulation for 150 ps under conditions of fixed backbone, followed by data collection over 300 ps.

Isothermal Calorimetry—The binding isotherms of Mg^{2+} to con-G and con-G mutants were determined by ITC measurements of the heat changes accompanying titration of Mg^{2+} into solutions of the relevant con-G sample. The titrations were performed with a Microcal (Northampton, MA) OMEGA titration calorimeter at 25 °C in a buffer of 10 mM Na-Mes, 100 mM NaCl, pH 6.5. Peptide samples ranging in concen-

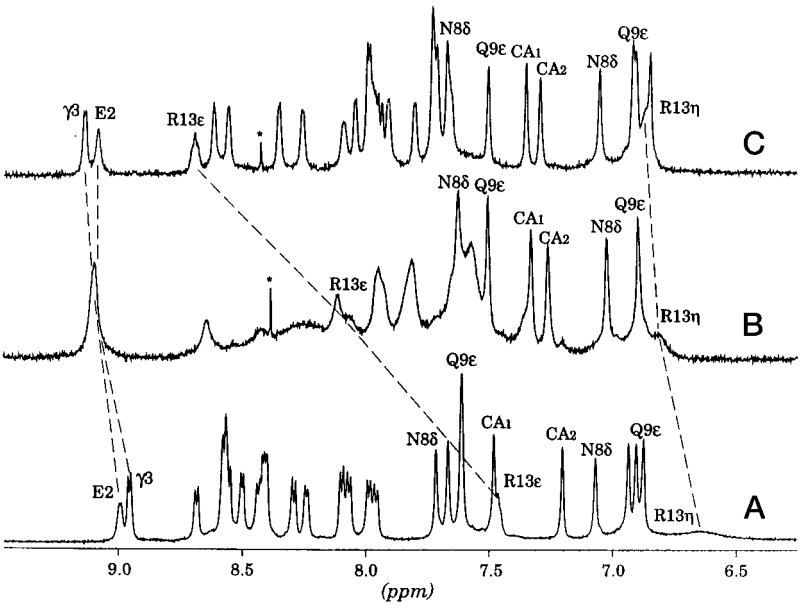

FIG. 1. **Amide region of the proton NMR spectra of con-G at pH 6.5 and 15 °C.** The peptide concentration was approximately 2 mM. *A*, apo-con-G; *B*, con-G in the presence of 40 mM Ca^{2+}; and *C*, con-G in the presence of 40 mM Mg^{2+}. The amide proton resonances of Glu^2 and Gla^3 were labeled with the one-letter code convention (γ = Gla) followed by the residue number. The resonances for several side-chain NH protons were also illustrated with the one-letter code and the residue number followed by the proton type. CA1 and CA2 represent the NH protons of the carboxyl-terminal amide group. An impurity signal is indicated by an *asterisk*. The broad features in the Ca^{2+}/con-G spectra remained the same with increased concentrations of Ca^{2+}, up to 100 mM.

trations from 0.23–1.0 mM (determined from quantitative amino acid analysis) in a total volume of 1.4 ml were placed in the reaction cell. After equilibration, an appropriate concentration of $MgCl_2$ (typically 30–50 times higher than that of the peptide solution) in matching buffer was delivered at discrete intervals, and the observed heat was measured after each injection. The total observed heat was corrected for the heat of dilution of the ligand by performing control titrations in the absence of peptide. The resulting titration curves were deconvoluted and inspected for the best-fit model using the ORIGIN for ITC software package supplied by Microcal.

Circular Dichroism—CD spectra of the con-G peptides as a function of metal ion concentration was monitored at 222 nm on an AVIV model 62DS spectrometer using a 1-cm path length cell. The relevant peptides were dissolved in a solution of 10 mM $NaBO_3$, 100 mM NaCl, pH 6.5, to a final concentration of 35 μM. The α-helical content of the peptides at various Mg^{2+} concentrations were calculated as described previously (31). The C_{50}Mg-CD values (the concentration of Mg^{2+} required to induce 50% of the alteration to the conformational change as determined by CD measurements) were determined by nonlinear least-squares fitting of the data using a Michaelis-Menten-type equation.

RESULTS

Interactions of Con-G with Ca^{2+} and Mg^{2+} Ions—The nature of the interaction of con-G with metal ions was assessed by use of one-dimensional ^{1}H NMR spectroscopy. Fig. 1 shows the effects of additions of Ca^{2+} and Mg^{2+} on the spectrum of apo-con-G. Here, it is seen that these cations influenced most of the αNH proton resonances of con-G. Both shifts and broadening (Fig. 1*B*) of the resonance peaks were noted in the presence of Ca^{2+} (all proton resonance assignments for apo-con-G and metal-loaded con-G are provided in Table S1a–c[2]). In the case of Mg^{2+}, the proton signals are also shifted, but they remain relatively sharp (Fig. 1*C*), therefore suggesting that Mg^{2+} has fully occupied its binding site(s) on con-G under the experimental conditions used (40 mM Mg^{2+} and 2 mM con-G). The dramatic shifts observed in apo-con-G as a result of Ca^{2+} and Mg^{2+} binding suggest that a conformational change in the peptide accompanies cation/con-G interactions.

The well-resolved two-dimensional ^{1}H NMR spectra of con-G allowed chemical shifts to be assigned to all of the protons of the peptide (Table S1a–c) and facilitated examination of the residue-specific effects of metal binding in the one-dimensional spectra (Fig. 1, *A–C*). In particular, the ϵNH resonance of Arg^{13} exhibits a very large downfield shift, from 7.5 to 8.1 ppm and to 8.7 ppm, as a consequence of Ca^{2+} and Mg^{2+} binding, respectively. Also, the extremely broad guanidino resonance in the apo-spectrum (Fig. 1*A*) narrows significantly in the metal-bound spectra (Fig. 1, *B* and *C*). Clearly resolved are the binding-induced shifts of the amide proton resonances for the side-chains of residues Asn^8 and Gln^9 and of the amide protons at the carboxyl terminus. Also notable are the large up-field shifts of the side-chain protons of residues that are incapable of metal binding, *viz.*, Leu^5, Leu^{11}, and Ile^{12} (Table S1a–c). These types of alterations, which are present throughout the peptide, indicate that global conformational reorientations occur in con-G upon binding of metal ions to this peptide.

Conformational Changes in Con-G Induced by Ca^{2+} and Mg^{2+} Binding—The secondary structure of con-G was investigated by two-dimensional ^{1}H NMR spectroscopy. All NMR observations on con-G indicate that this peptide has no defined secondary structure in the absence of divalent cations. Initial evidence in support of this point originates from the αCH chemical shifts values, an approach commonly used to qualitatively identify secondary structural elements in peptides and proteins (32). Because there are no reported random coil values for the Gla residue, and because these chemical shifts would be expected to be sequence-dependent in the random coil state, the αCH proton chemical shifts of con-G determined in 6 M urea were used as the reference random coil values. The fact that four or more residues, without disruptions, do not experience upfield or downfield shifts of 0.1 ppm or greater when compared with the random coil values suggests that there is no dominant secondary structure (Fig. 2). In addition, the temperature coefficients of the backbone chemical shifts for apo-con-G were determined through a series of TOCSY spectra acquired at 5° intervals from 5 °C through 30 °C. A temperature coefficient in the range of −6 to −9 ppb/K was found for all backbone αNH protons of apo-con-G. These values are consistent with random coil conformation and suggest no preference for the backbone hydrogen bonding that exists in a helical state.

Consistent with the chemical shift values, NOE patterns also suggest that the peptide backbone of apo-con-G does not fold in any preferred structural arrangement. Fig. 3*A* provides a summary of NOE values observed for con-G in the absence of divalent metal ions. Except for intraresidue and sequential NOEs, neither long-range nor medium-range NOE contacts were observed at sample temperatures of 15 or 25 °C. Even at a lowered temperature of 5 °C, there were only three very weak

[2] Supplementary Tables S1a–c and S2 are available from the corresponding author.

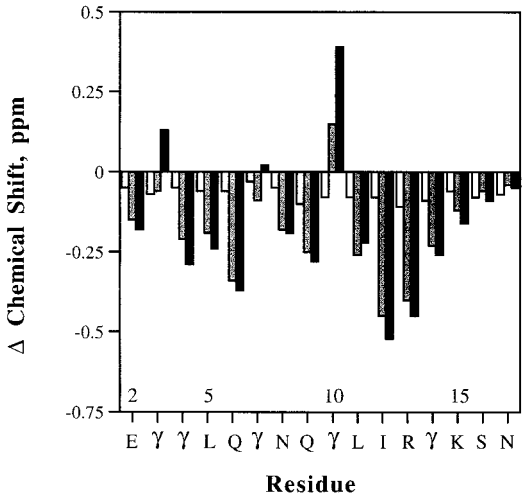

FIG. 2. **Conformational shifts of the αCH protons for con-G in the absence and presence of divalent cations.** The *open bars* refer to apo-con-G; the *gray bars* refer to apo-con-G in the presence of 40 mM $CaCl_2$; and the *black bars* refer to apo-con-G in the presence of 40 mM $MgCl_2$, at pH 6.5 and 15 °C. The chemical shift differences were calculated through subtraction of the corresponding shifts obtained for apo-con-G in 6 M urea from the measured values.

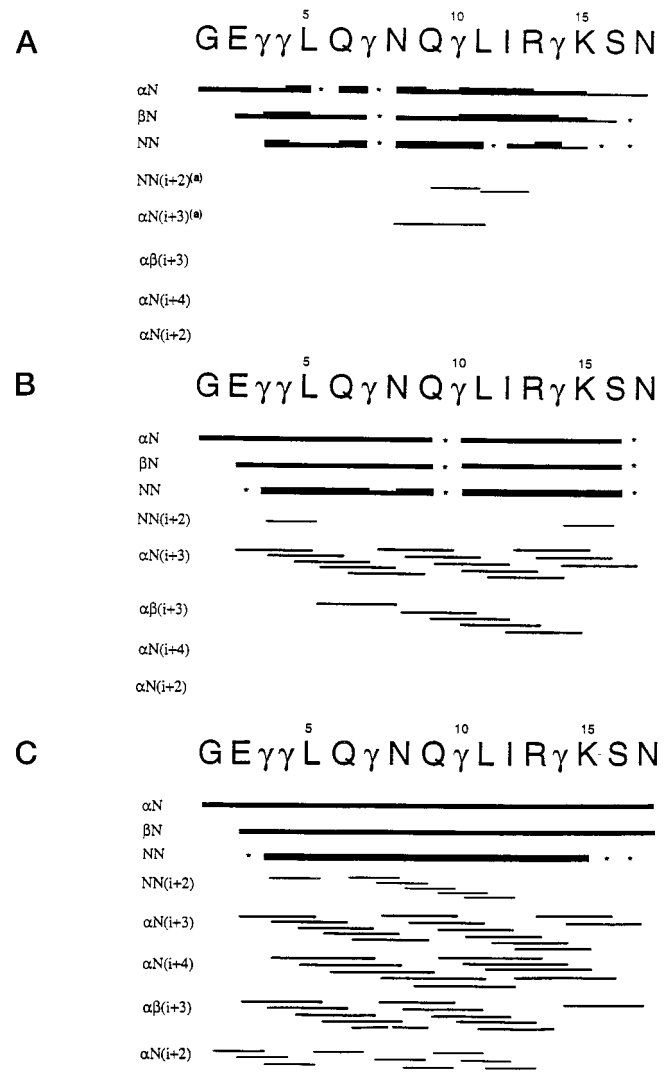

FIG. 3. **Summary of the sequential and medium-range NOE connectivities observed for con-G at pH 6.5.** *A*, apo-con-G; *B*, con-G with Ca^{2+}; *C*, con-G with Mg^{2+}. The thickness of the *bars* provides a qualitative measure of the strength of the NOE cross peaks. An *asterisk* indicates that the assignment of the observed cross peak was ambiguous due to resonance overlaps. The NOE summary for con-G with Ca^{2+} was obtained at 25 °C because of broad proton signals at low temperature (Fig. 1*B*). The NOE connectivities for apo-con-G and con-G with Mg^{2+} were a combination of NOEs observed at different temperatures (5, 15, and 25 °C). These NOEs observed for apo-con-G are very weak and only appeared in the NOESY spectrum at a temperature of 5 °C.

medium-range NOEs between the αNH protons of residues Gln^9 and Leu^{11} and residues Leu^{11} and Arg^{13} (i, i + 2), and between the αCH proton of Asn^8 and the αNH proton of Leu^{11} (Fig. 3*A*). Additionally, $^3J_{HN\alpha}$ coupling constants were found to be approximately 7 Hz for all residues of apo-con-G (Table I), again consistent with a peptide with no dominant conformation.

In contrast to apo-con-G, all NMR parameters of con-G in the presence of Ca^{2+} or Mg^{2+} indicate that the peptide possesses a substantial metal cation-induced α-helical structure. Large negative values of deviations of the αCH proton chemical shifts were seen for most residues in the presence of either Ca^{2+} (Fig. 3*B*) or Mg^{2+} (Fig. 3*C*). Of special note, >0.2-ppm shifts were observed for seven amino acid residues in con-G in the presence of Ca^{2+} and for nine residues in the presence of Mg^{2+}. Positive values for the αCH conformational shifts were detected for some of the Gla residues, *viz.*, Gla^{10} in the presence of Ca^{2+}, and Gla^3, Gla^7, and Gla^{10} in the presence of Mg^{2+}. However, because these positive values only occur for Gla residues, they likely reflect direct metal ion binding effects, rather than the conformations at these residues.

The NOE connectivities of Ca^{2+}-bound con-G are summarized in Fig. 3*B*. Due to line broadening, the resonances could not be assigned unambiguously at lower temperatures (≤15 °C). Thus, the NOEs shown in Fig. 3*B* were obtained at 25 °C. Even with sharper signals at the higher temperature, some expected NOEs were not observed or could not be unambiguously assigned. Despite this, many NOEs characterizing an α-helical structure were identified. For example, strong sequential NOEs between the αNH protons were detected for amino acid residues 3 to 9 and for residues 10 to 16. The missing NOE contacts between the backbone amide protons of residues 2 and 3, 9 and 10, and 16 and 17 are due to resonance overlap in these cases. However, there were many (i, i + 3) NOE contacts between the αCH and the αNH protons of the same residues in Ca^{2+}/con-G. Furthermore, five (i, i + 3) NOE connectivities between αCH and βCH protons were found, providing additional NOEs characteristic of an α-helical structure.

The NOE patterns of con-G in the presence of Mg^{2+} are illustrated in Fig. 3*C*. The observed NOEs fully characterize an α-helical structure. Because of relatively sharp proton resonances with Mg^{2+}, it was possible to assign many sequence-specific NOEs that were not observable in the case of Ca^{2+}. The α-helix appears to extend from the amino terminus to carboxyl terminus of the peptide. This is supported by the expected (i, i + 3) NOE connectivities, including αN(i, i + 3) and αβ(i, i + 3). In addition, NOE contacts between protons of αN(i, i + 4) and αN(i, i + 2) were found for many pairs of residues. The fact that the NOE intensities are much higher for αN(i, i + 4) than for αN(i, i + 2) is an indication of that the metal ion-induced conformation of con-G is mainly an α-helix.

Values of $^3J_{HN\alpha}$ coupling constants also support the α-helical conformation for Mg^{2+}-loaded con-G (Table I). Small values (<5.5 Hz) of these coupling constants were detected for residues 3 to 5, 8, and 9 and for residues 11–16. Values of ≈6 Hz were found for residues 2, 6, 7, and 17. Only one relatively large value (≈7 Hz) was observed for residue 10. Also, the temperature coefficients of amide proton chemical shifts for Mg^{2+}/con-G were estimated from a series of TOCSY spectra accumulated in a temperature range of 5–30 °C. Very small values (<4 ppb/K) of the temperature coefficients were observed for the αNH

protons of residues 5–17, with the only exception being Asn^8 (≈7 ppb/K). Such small values of the chemical shift temperature coefficients indicate that these backbone amide protons are potential candidates for hydrogen bonding.

The Solution Structure of Con-G in Complex with Mg^{2+} Ions—Because binding of Ca^{2+} and Mg^{2+} induces similar conformational changes in con-G, detailed structure investigations were only performed for the Mg^{2+}/con-G complex, utilizing the more extensive set of NMR parameters observed, with assignments facilitated as a result of the sharp and well resolved proton resonances of con-G in the presence of Mg^{2+} ions. In addition to an α-helical backbone, the conformations for the side-chains of Mg^{2+}/con-G appear to be also well defined, especially those for residues 4–14, as indicated by the many backbone/side-chain and side-chain/side-chain NOE contacts among these residues. For example, in addition to $\alpha\beta(i, i + 3)$ NOE contacts observed for most pairs of residues (Fig. 3*C*), backbone/side-chain NOE connectivities were found between the proton pairs of Leu^5-αCH and Asn^8-δNH, Asn^8-αCH and Leu^{11}-CH_3, Gla^{14}-αNH and Gla^{10}-γCH, Asn^8-αNH and Leu^5-CH_3 (Fig. 4). Furthermore, both the αCH and αNH protons of Gln^9 have NOE connectivities to the methyl protons of Ile^{12}. The αCH protons of Gla^{14}, Lys^{15}, and Asn^{17} were found to be in contact with the protons of the carboxyl-terminal amide group. Besides these backbone/side-chain NOE contacts, NOE connections between side-chain protons were detected for the proton pairs of Gla^3-γCH and Gla^7-γCH, Asn^8-δNH and Ile^{12}-CH_3, Asn^8-δNH and Gla^4-βCH, and Gln^9-ϵNH and Leu^5-CH_3.

The resonance characteristics of the side-chain NH protons of Arg^{13} are particularly noteworthy. In apo-con-G, a normal chemical shift was found for the ϵNH proton (Fig. 1*A*). When con-G was loaded with Ca^{2+} or Mg^{2+}, the resonance for this proton was shifted >1 ppm downfield (Fig. 1, *B* and *C*). In addition, the temperature coefficient for this proton is very small (<4 ppb/K), indicating that it is a potential hydrogen bonding candidate. Possible partners for this hydrogen bond interaction could be the Gla^{10} backbone or the side-chain carbonyl groups of Gla^{10} and Gla^{14}, because NOE connectivities were observed between the ϵNH proton of Arg^{13} to the αCH protons of Gln^9 and Gla^{10} and to the γCH proton of Gla^{14} (Fig. 4). A weak NOE was also found between Arg^{13}-ηNH and Gla^{14}-γCH. Those observed NOEs place the side-chain of Arg^{13} in a position in close contact with those of Gla^{10} and Gla^{14}.

The Mg^{2+}-induced structure of con-G was calculated from 191 distance constraints, including 60 intraresidue, 49 sequential, and 82 of medium range (Table S2). One hundred initial structures were generated by distance geometry calculations using only backbone NOEs. Thirty of these structures with low constraint violations were chosen for further structure optimization by combining backbone NOEs with additional side-chain/side-chain NOE constraints. The initial structures also allowed the assignment of some overlapped NOEs. Because the exact position of the bound Mg^{2+} ion was not known at this stage, full energy minimization was not performed on the NMR-based structural model because excluding bound cation would have led to a poor definition of the metal-dependent conformation. Fig. 5 illustrates 15 structures thus obtained with their backbone atoms superimposed. This cluster of structures possess root mean square deviation values of 0.46 Å for backbone atoms and 1.1 Å for all heavy atoms. The average structure for Mg^{2+}/con-G is provided in Fig. 6. Here, it was observed that the major subpopulation of structures of con-G in complex with Mg^{2+} is represented by an α-helix that spans the entire length of the peptide.

TABLE I
$^3J_{HN\alpha}$ coupling constants

Residue	apo-conantokin-G	Ca^{2+}-conantokin-G
Glu^2	6.9	6.3
Gla^3	6.6	5.4
Gla^4	6.7	5.4
Leu^5	6.7	5.4
Gln^6	6.7	6.3
Gla^7	6.7	6.3
Asn^8	6.7	5.4
Gln^9	6.7	5.4
Gla^{10}	6.7	6.9
Leu^{11}	6.6	5.4
Ile^{12}	6.5	5.4
Arg^{13}	6.6	5.4
Gla^{14}	6.7	5.4
Lys^{15}	6.7	5.4
Ser^{16}	6.6	5.4
Asn^{17}	7.4	6.3

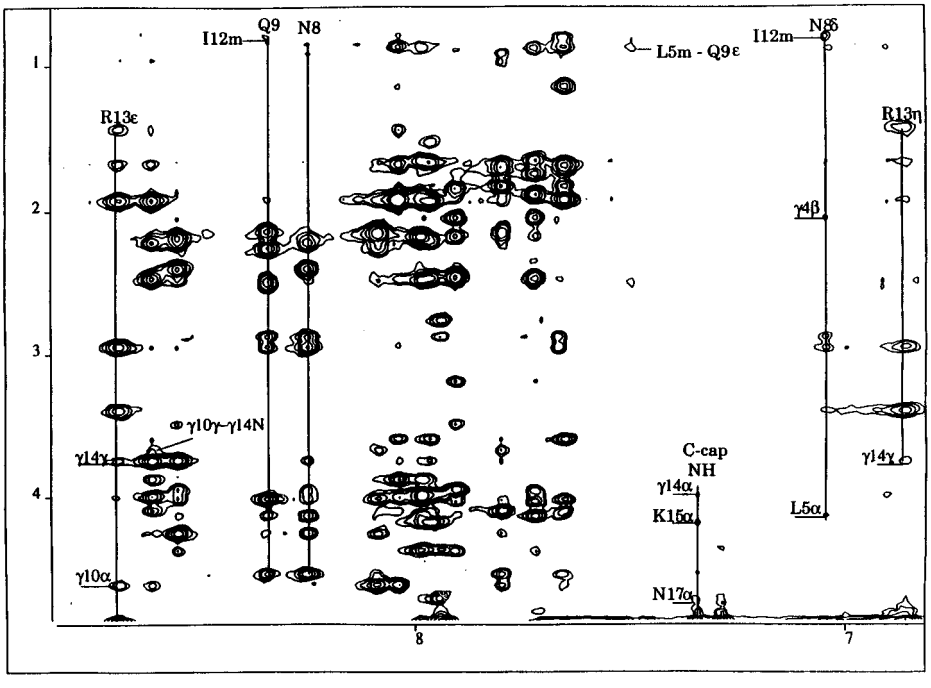

FIG. 4. **A portion of the two-dimensional NOESY spectrum for con-G in the presence of Mg^{2+}.** Data were collected at 15 °C with a mixing time of 250 ms. The sample conditions were 2 mM for the peptide and 40 mM for $MgCl_2$, pH 6.5, in a buffer solution containing 10 mM sodium borate and 100 mM NaCl. Several backbone and side-chain NH resonances are illustrated along with long-range NOE connectivities. The weak long-range NOEs were also reproducibly observed in the NOESY spectra acquired at 5 °C.

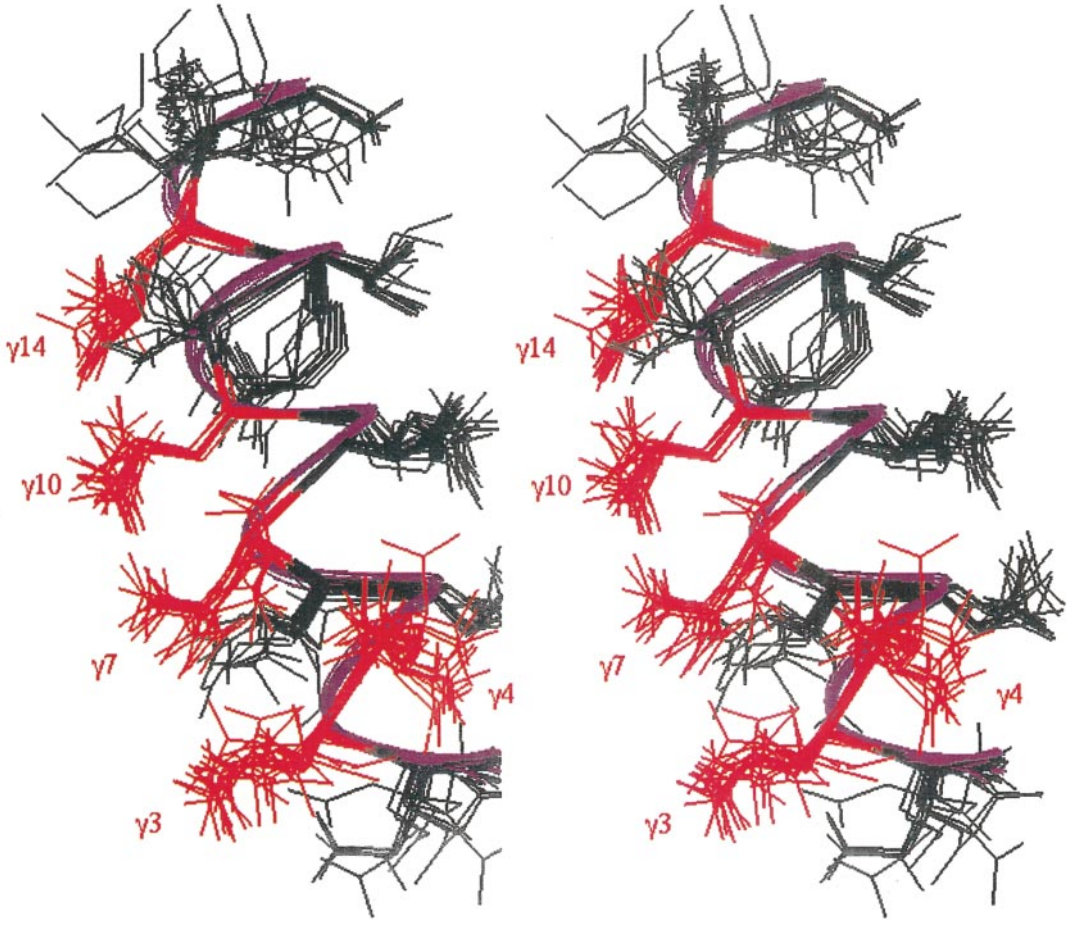

FIG. 5. **Stereo view of a cluster of 15 converged structures for Mg^{2+}/con-G derived form distance geometry calculations.** The individual conformations were superimposed on backbone α-carbon atoms. The side-chains for Gla^3, Gla^4, Gla^7, Gla^{10}, and Gla^{14} are labeled and are colored *red*. The clusters possess root mean square deviation values of 0.46 Å for backbone atoms and 1.1 Å for all heavy atoms.

Docking of Mg^{2+} in Con-G—The most probable locations of the Mg^{2+} ions in the con-G complex were identified using the genetic algorithm-molecular dynamics simulation procedure that has been successfully applied to even more complex structures of this type. For this procedure, a three-Mg^{2+}/con-G binding model was applied with two Na^+ ions added to balance charge. The three-step procedure (initial placement of the Mg^{2+} ions at each of the many possible oxygen-oxygen midpoints, application of the genetic algorithm to locate the lowest energy structure of all possible placements in which the ions move, and finally, molecular dynamics on the solvated lowest energy form in which the ions and side-chains have their geometries energy-optimized) resulted in a final coordination pattern for which a Mg^{2+} ion is coordinated to three oxygens from Gla^{10} and Gla^{14}, another Mg^{2+} ion is coordinated to two oxygens of Gla^7, and the final ion is coordinated to oxygens from Gla^3, Gla^4, and Gla^7. The genetic algorithm procedure was repeated several times with different genetic algorithm parameters, always with the same result. A two-Mg^{2+} site model was also subjected to the molecular dynamics minimization, but the final model poorly predicted the Mg^{2+} binding results of the mutants. The average structure generated from the resulting coordinates is shown in Fig. 7.

Binding of Mg^{2+} to Con-G Mutants—To test the roles of individual Gla residues in Mg^{2+} binding using the models proposed for the Mg^{2+} con-G complex, binding isotherms were determined for Mg^{2+} in synthetic con-G-derived peptides wherein each Gla residue was altered to Ala. The method employed for these determinations was ITC, in which the heat changes in con-G accompanying Mg^{2+} binding were measured and deconvoluted into thermodynamic characteristics of the binding. A typical example of the binding isotherm obtained for wild-type con-G is provided in Fig. 8. The data for all of the mutants are of this same high quality. The resulting values of the stoichiometry and K_d values that characterize Mg^{2+} binding to each of the mutant peptides generated in this report are summarized in Table II. It is seen from this list that one tight site and at least one weaker site, of K_d 10-fold greater than the tight site, exist in the wild-type peptide. All mutants only possess a single measurable Mg^{2+} site. The tight site is not present in the Gla^4Ala, Gla^{10}Ala, and Gla^{14}Ala mutants, and the weak site is not detectable in the remaining variants. Con-G[D-$Gla^{3,4,7,10,14}$], a peptide lacking secondary structure as measured by CD[3] was also examined by ITC. This con-G variant did not display an isotherm over the upper range of Mg^{2+} concentrations employed in this study, suggesting that the folded peptide, and not discrete Gla residues or dyads, is responsible for enforcing the metal binding loci. Although ΔH values that characterize these interactions were also obtained, we chose not to base any interpretations of the Mg^{2+}/con-G binding characteristics on these values. This is because the heats of reaction also likely contain contributions from heats associated with the refolding of the peptides. Because there was no way to separate these two phenomena at this stage, the ΔH values associated strictly with cation binding could not be

[3] T. Blandl and F. J. Castellino, unpublished results.

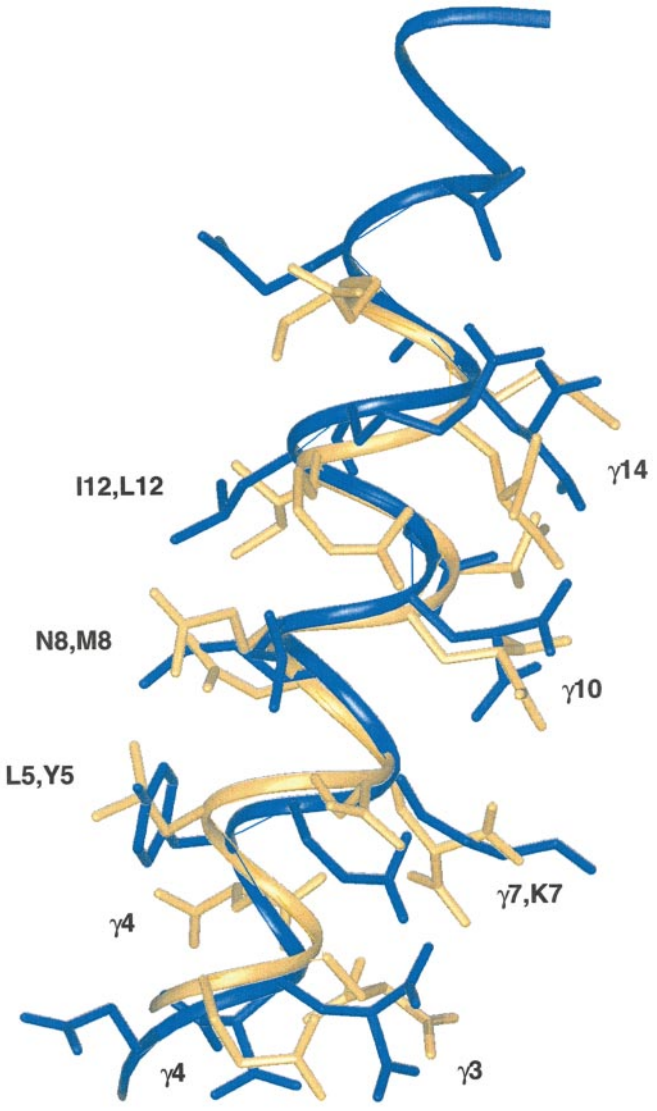

FIG. 6. **Comparison of the average structures of Ca^{2+}/con-T and Mg^{2+}/con-G.** The backbones of con-G (*gold*) and con-T (*blue*) in these metal complexes were superimposed on the α-carbon atoms of residues 1–17. Certain side-chains of interest are labeled. When two such indications are made for overlapping residues, the first designation is for con-G and the second is for the corresponding residue in con-T.

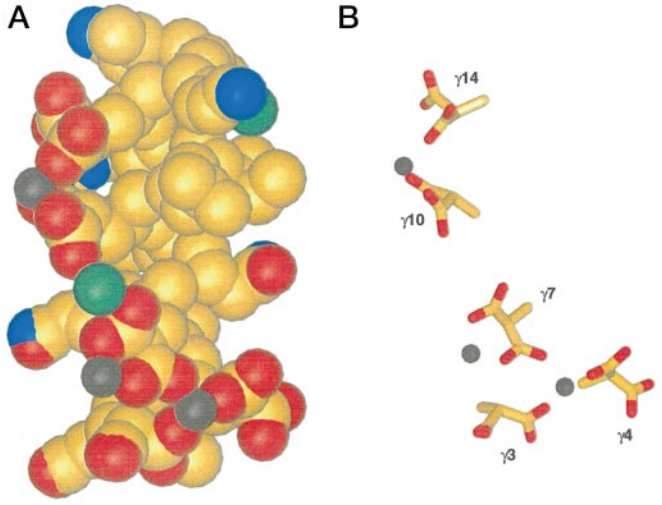

FIG. 7. **The Mg^{2+}-loaded energy minimized structure of con-G.** A total of three Mg^{2+} ions (*black*) were docked in this structure using the genetic algorithm, beginning with the NMR-derived coordinates of con-G loaded with Mg^{2+}. The structure was then refined by molecular dynamics simulation. In this illustration, the side-chains (from the β-carbons) of all amino acid residues of con-G are illustrated, and certain residues are labeled. All side-chain carbon atoms are shown in *orange*, nitrogens are *blue*, and oxygen atoms are *red*. *A*, space-filling representation. *B*, the relationships between side-chain residues implicated in binding to Mg^{2+} and the Mg^{2+} ions. The orientation is as in *A*. The representations in *A* and *B* are not on the same scale.

determined. However, this consideration does not affect determination of the K_d values by this method because saturable titrations were observed, and only the incremental heat changes accompanying Mg^{2+} addition, not their absolute values, were required.

Mg^{2+} induces a large conformational alteration in con-G, and the functions of individual Gla residues in promoting the binding required for this change were examined by CD analysis of the con-G mutants in the presence and absence of Mg^{2+}. For this analysis, the effects of Mg^{2+} on the molar ellipticities of the peptides at 222 nm were determined, because a wavelength of 222 nm would effectively monitor alterations in the α-helical conformations of the peptides. Examples of the titrations for wild-type con-G and the mutant, con-G-Gla^3Ala, are displayed in Fig. 9. The relative propensities of the peptides to adopt the Mg^{2+}-induced conformational changes are quantitatively compared in Table II by determinations of the concentration of Mg^{2+} required to induce 50% of the alteration to the α-helical conformation (C_{50}Mg-CD). Here, it is seen that mutation of any Gla residue diminishes the capacity of con-G to adopt its full α-helical conformation. Interestingly, the Gla^3Ala, Gla^7Ala, and Gla^{10}Ala mutants require less Mg^{2+} than the wild-type peptide to induce the conformational change, whereas Gla^4Ala and Gla^{14}Ala require greater levels of Mg^{2+} for the change to occur.

DISCUSSION

Conformational Stabilities of the Conantokin Peptides—Despite the relatively high sequence homology of con-T and con-G (80% for Gla residues and 30% for all residues), they are structurally diverse in their apo-forms. Con-T is nearly fully α-helical in the absence of divalent metal ions (11). Con-G exists primarily as an unstructured peptide in aqueous solution with some local structures, indicated by a few weak nonsequential NOEs (Fig. 3*A*). However, these differences in the apo-structures can be explained by an analysis of the interactions of the side-chains at the (i, i + 3) and (i, i + 4) positions. Con-T contains many of the side-chain/side-chain interactions that stabilize α-helical conformations in peptides, namely hydrophobic, electrostatic, charge-helix-dipole, end-capping, and hydrogen-bonding contacts (11). Con-G lacks appropriately spaced hydrophobic residues and has only a few potential salt bridges and ion pairs. Inspection of the central portion of the helices, the region most important for structural stability, reveals that con-T has an extensive (i, i + 3) and (i, i + 4) electrostatic network, involving residues Gla^3-Lys^7-Gla^{10}-Arg^{13}-Gla^{14}-Lys^{18} (11), whereas con-G has several potential electrostatic repulsions, *viz.*, Gla^3-Gla^7-Gla^{10}-Gla^{14} (Fig. 6). Although both peptides have a potential Gln^6-Gla^{10} hydrogen bond and an Arg^{13}-Gla^{14} ion pair, interactions that are believed to be important for the stability of the apo-con-T α-helix, the presence of a Gla^7 in con-G may be severely destabilizing. In addition, con-T has a hydrophobic cluster (Tyr^5-Met^8-Leu^9-Leu^{12}) that likely contributes to the stability of the electrostatic interactions (11). The corresponding residues in con-G are Leu^5, Asn^8, Gln^9, and Ile^{12}, with two polar residues in positions 8 and 9 breaking the hydrophobic cluster (Fig. 6). Thus, the drastic difference in α-helicity between these peptides provides strong evidence that

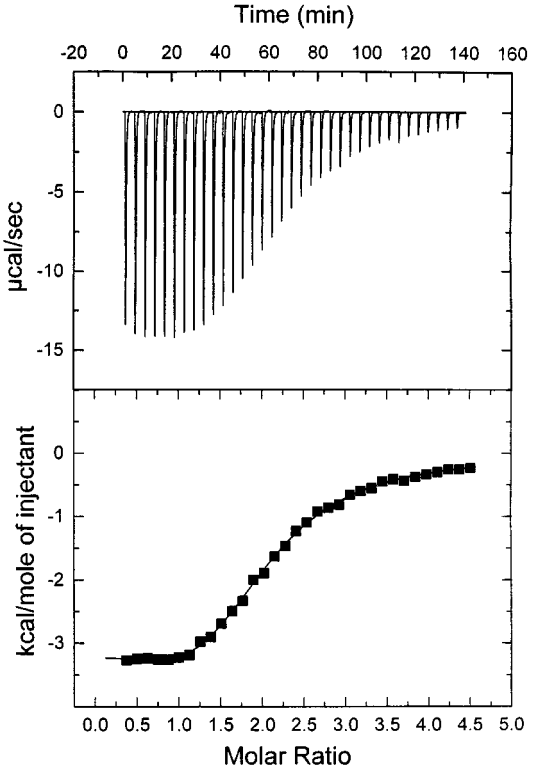

FIG. 8. **The binding of Mg^{2+} to con-G.** The effects of the addition of Mg^{2+} on the heat changes of con-G were determined by ITC. *Top*, incremental heat changes accompanying titration of con-G with Mg^{2+} at 25 °C. A sequence of 3-µl injections from a stock solution containing 40 mM $MgCl_2$ was added to the sample cell containing 690 µM con-G. The buffer was 10 mM Na-Mes, 100 mM NaCl, pH 6.5, at 25 °C. Each injection took place over a 10-s time interval, with 2 min between injections. The cell volume was 1.40 ml. *Bottom*, the heat changes per mole of Mg^{2+} injected are plotted against the molar ratio of Mg^{2+} to con-G. The line is the best-fit of the data to a binding isotherm characterized by $n_1 = 1.0$, $K_{d1} = 20$ µM, $\Delta H_1 = -3.18$ kcal/mol; $n_2 = 0.97$, $K_{d2} = 286$ µM, $\Delta H_1 = -4.69$ kcal/mol.

TABLE II
Properties of the Mg^{2+}/con-G and mutant con-G peptides

Peptide	α-Helix[a]	C_{50}Mg-CD[b]	n[c]	K_d[c]
	%	µM		µM
con-G	2 (73)	120	0.97	20
			1.02	286
Gla^3Ala	5 (44)	58	1.08	34
Gla^4Ala	0 (59)	240	0.69	186
Gla^7Ala	5 (32)	38	0.84	17
Gla^{10}Ala	7 (31)	100	1.04	111
Gla^{14}Ala	11 (39)	430	0.95	544

[a] The initial (and final) α-helical content from analysis of the CD changes.

[b] The total concentration of Mg^{2+} required for 50% of the conformational change as determined from CD measurements.

[c] The stoichiometry (n) and dissociation constant (K_d) that characterize the binding of Mg^{2+} to the indicated peptides as determined from ITC measurements. The reported n and K_d values represent the average of two experiments and did not deviate by more than 15% between experiments.

side-chain/side-chain interactions can contribute significantly to α-helix stabilization, despite the unfavorable entropic contributions consequent to immobilizing the conformation of the side-chain atoms in the α-helix.

In contrast, a recent contribution has appeared in which it was concluded from ^{1}H NMR structural analysis that apo-con-G contained a high degree of helical structure (7). This observation is at variance with previous CD (6) and Fourier transformed-infrared (2) studies, which showed that apo-con-G was essentially structureless. It is possible that these differences arise from the use of a limited number of medium- to long-range NOEs and the employment of $^3J_{HN\alpha}$ coupling constraints as input for structural calculations.

Metal Ion Binding Sites in Con-G—Many cations, including Ca^{2+} and Mg^{2+}, induce α-helical conformations in con-G (6, 9) and increase the existing α-helicity in con-T (6). The Gla residues, which are known to bind to Ca^{2+} and other divalent and trivalent cations when present in proteins, are the most likely candidates for metal ion coordination in the conantokins. Ca^{2+} titrations, employing a Ca^{2+}-selective electrode, revealed that con-G possessed 2–3 metal binding sites (6). Similar values were obtained for Mn^{2+} by EPR titrations (33) and for Mg^{2+} by the ITC experiments described in the current report (Fig. 8 and Table II). Despite the similarity between the number of Mg^{2+} and Ca^{2+} sites inferred from a variety of biophysical techniques, there is a significant difference in the affinities of these metals for con-G. The weak (K_d = 2–3 mM) Ca^{2+} binding (6) likely results in an exchange phenomenon that is slow on the NMR time scale and that is manifest by excessive line broadening (Fig. 1*B*). Furthermore, the broad αNH resonances in the Ca^{2+}/con-G spectrum became sharper at a higher temperature of 25 °C (data not shown), another indication of broadening by conformational exchange among Ca^{2+}-free and Ca^{2+}-loaded forms. It does not appear that aggregation of the peptide is an adequate explanation of the observed resonance line widths, because not all of the αNH protons of con-G exhibited spectral broadening as a result of Ca^{2+} binding (Fig. 1*B*). In addition, previous data obtained with both con-G and con-T demonstrated that Ca^{2+}-induced aggregation of these apo-peptides did not occur under these conditions (6).

The impetus for solving the Mg^{2+}-loaded con-G peptide structure stems from the obvious biological relevance of the Mg^{2+} ions in relation to the NMDA-R and from the availability of high quality experimental data that allows for a detailed conformational analysis that is not possible in the presence of Ca^{2+}. The observation of a full peptide-spanning α-helix from this current NMR study is a conclusion that contrasts somewhat with the structure recently reported for Ca^{2+}-induced con-G conformation. In this latter case, some subpopulation of 3_{10}-helical structures was proposed (9). The most likely reason for these differences is that many characteristic NOEs for an α-helical structure were not observed in these studies due to broad proton resonances of con-G in the presence of Ca^{2+}. In contrast, the backbone of the Mg^{2+}-dependent con-G average structure is clearly well-defined by the NOE-driven structural analysis because many NOEs were observed among both the backbone and the side-chain protons (Figs. 3*C* and 4).

Due to well-defined side-chains in the NMR-derived solution structure of Mg^{2+}-loaded con-G, the location of metal binding sites can be credibly proposed. The spatial proximity of Gla^{10} and Gla^{14} in the solution structure (Figs. 5 and 6) suggests that they may constitute one of the metal binding locations. It is interesting to note that the Gla^{10} and Gla^{14} are conserved in con-T and con-G. A single strong metal binding site exists in con-T, as reported previously (6), along with a possible weaker site. This lone strong metal ion binding site in con-T is coordinated by the side-chains of Gla^{10} and Gla^{14}, as revealed from molecular dynamics simulations and from analysis of variant con-T-based peptides (12). The clustering of Gla^3, Gla^4, and Gla^7 in con-G suggests that metal ions may also bind at a site involving these residues.

^{1}H NMR chemical shifts can provide some evidence for which residues are involved in binding to the metal ions. For example, binding of divalent metal ions may induce chemical shift variations of the γCH protons of Gla residues. In fact, compared

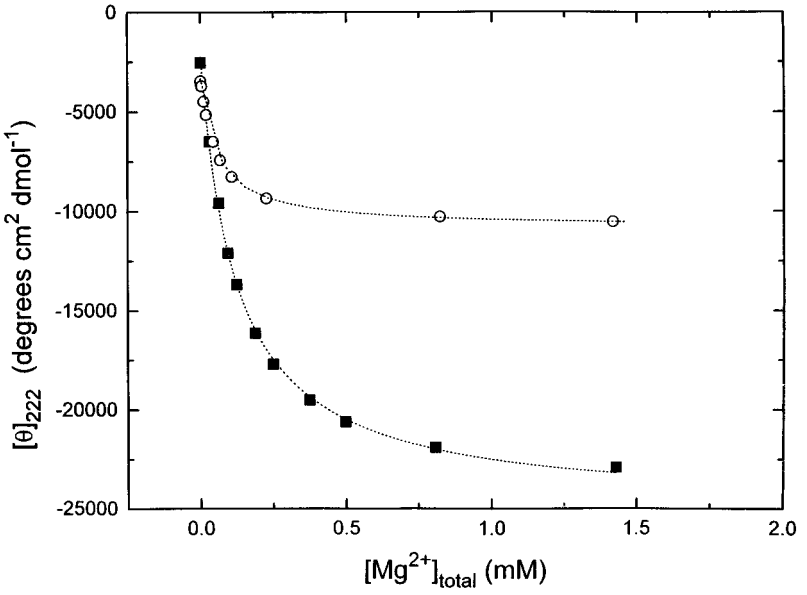

FIG. 9. **Circular dichroism titrations of con-G with Mg^{2+}.** The effects of titration with Mg^{2+} on the α-helical contents of apo-con-G (■) and con-G-Gla^{3}Ala (○) were determined by titration with metal ion. The values of the molar ellipticities at 222 nm are plotted against the total Mg^{2+} concentrations. The buffer was 10 mM Na-Mes, 100 mM NaCl, pH 6.5, at 25 °C.

with the Mg^{2+}-free form (Table S1a), large downfield shifts (ranging from 0.4 to 0.6 ppm) were observed for the γCH protons of Gla^3, Gla^7, Gla^{10}, and Gla^{14} in the Mg^{2+}-loaded state (Table S1c). These observations indicate that the environments for these γCH protons are quite different between apo-con-G and the Mg^{2+}/con-G complex. On the other hand, there is a smaller change for the γCH proton of Gla^4 upon metal biding, suggesting that it is minimally involved in such binding, as was the case for Ca^{2+} binding to con-T (12). Furthermore, there are large and positive deviations for the αCH chemical shifts of Gla^3, Gla^7, and Gla^{10} (Fig. 2*C*). A downfield shift of αCH proton resonances, relative to those for the random coil conformation, is usually an indication of an extended conformational state. However, these changes could be due to the local effects induced by the bound cations because all other NMR parameters indicate that α-helix disruption does not likely occur in the Mg^{2+}/con-G complex. Because these types of experiments do not localize the metal ion binding site any more exactly, we undertook an additional modeling approach for this purpose.

Localizing the Mg^{2+} Binding Sites in Con-G—For predictions of the locations of Mg^{2+} binding sites in con-G, the genetic algorithm-molecular dynamics simulation methodology was employed, because that approach has proved to accurately predict cation binding sites in even more complex peptides, such as the Gla domain of coagulation fIX (28). To maximize its predictive power, the peptide coordinates employed for initial calculations were those from the NMR-derived structure of the Mg^{2+}/con-G complex. Although the direct Mg^{2+} binding data with wild-type con-G were more consistent with a two-site *versus* a three-site cation:peptide model, the latter was chosen for further elaboration because the NMR analysis of con-G and the direct binding data with the mutant peptides were more suggestive of this model.[4] Specifically, the two site model eliminated Gla^{14} from coordination of Mg^{2+}, and this was inconsistent with Mg^{2+}/mutant peptide binding data (Table II). Additionally, the NMR data show clear chemical shift changes of the γCH proton of Gla^{14} upon addition of either Ca^{2+} or Mg^{2+} (Table S1a–c). Thus, we propose the model in Fig. 7 as one that fits the majority of other experimental evidence. In this case, one Mg^{2+} ion is coordinated by γ-carboxylate oxygen atoms of Gla^3, Gla^4, and Gla^7; another only by those of Gla^7; and a third by γ-carboxylate oxygen atoms of Gla^{10} and Gla^{14}. The locations of the Ca^{2+} ions in con-T (12) and of the Mg^{2+} ions in con-G are somewhat different. Not insignificant in determining this distribution is Gla^7, a residue not present in con-T. This side-chain provides a coordination site for a Mg^{2+} ion that is also shared by Gla^3 and Gla^4. In the case of con-T, wherein Gla^4 does not appear to participate in metal binding, the side-chain carbonyl oxygen at Gln^6 serves as a donor residue for one Ca^{2+} ion, along with the Gla^3 γ-carboxyl oxygen (33). Thus, it appears as though the presence of Gla^7 has the effect of involving Gla^4 in cation binding in con-G. The other Ca^{2+} ion bound to con-T is coordinated by only the Gla^{10} and Gla^{14} side-chain oxygen atoms (12). Similarly, the model of Mg^{2+} binding to con-G appears to allow one ion be coordinated by these same side-chain atoms. Finally, if another weak Mg^{2+} site exists in con-G and, as discussed above, the direct binding data is ambiguous in that regard, its donor oxygen atoms would originate from each of the γ-carboxylate oxygen atoms of Gla^7. This would be expected to be a very weak binding site, as suggested from Ca^{2+}-selective electrode titrations of malonic acid which yielded a K_d for Ca^{2+} of 4.5 mM.[5]

The α-Helical Structure as the Bioactive Conformation—Ca^{2+} and Mg^{2+} play critical roles in NMDA-R function; Ca^{2+} is the cation transported through the open channel, and a Mg^{2+} site on the receptor plays an important role as a voltage-dependent channel blocking agent (34, 35). Thus, studies of binding of these cations to other NMDA-R agonists and antagonists are especially relevant. Con-G binds tightly to the NMDA-R (5). Such high avidity would not be expected of a small and loosely structured peptide, such as con-G, because its conformational equilibrium mixture likely includes many inactive conformer species. The elimination of a significant population of inactive conformations, through metal-dependent α-helical induction,

[4] It should be noted that the detection of two metal binding sites in con-G as determined by isothermal calorimetry under our working concentrations of peptide (<1 mM) does not rule out the existence of additional site(s) too weak to be detected by this method. As discussed previously (34) the product of the binding constant and the concentration of the macromolecular component of the titration must lie between 1 and 1000 in order to obtain an isotherm from which a precise value for the binding constant can be extracted. As such, a weak binding site characterized by a K_d of approximately 5 mM (K_a = 200 M^{-1}) would necessitate peptide concentrations of greater than 5 mM for the generation of useful isotherms. Such experiments not only are limited by the availability of peptidic material but also may be hindered by metal-induced peptide aggregation at these very high concentrations.

[5] M. Prorok and F. J. Castellino, unpublished data.

might be expected to facilitate tighter receptor binding. This is especially relevant when the conformational stabilizing elements are critical components of the physiological milieu and are as important to the function of the NMDA-R as are Ca^{2+} and Mg^{2+}. For example, it has been shown that 30-μl intracerebral injections of a 150 μM con-G solution into pre-2-week-old mice are sufficient to induce a deep and prolonged sleep-like state in these subjects (6). Assuming a peptide dilution factor of 10-fold arising from a brain volume of 300–500 μl[6] and a cerebrospinal fluid concentration of Mg^{2+} of 1.5 mM, this would lead to essentially 100% occupancy of the tight Mg^{2+} site (K_d = 20 μM) of con-G and about 80% occupancy of the weaker site (K_d = 285 μM). Under these bioassay conditions, con-G clearly predominates in its metal-bound, highly α-helical conformation, strongly suggesting the primacy of this structured form in mediating the observed physiological effects.

In a previous study, the NMR solution structure of apo-con-T was solved (11). The data were consistent with a structure composed of a α-helix spanning the entire length of the peptide with well-defined backbone and side-chain orientations, due to the existence of many favorable interactions optimal for stabilization of the α-helix. Based on the well folded nature of apo-con-T α-helix, it was further considered that the α-helical structure would be the bioactive conformation, because denaturing an α-helix by subsequent receptor binding would be energetically unfavorable. In the present study, con-G, a peptide with similar NMDA-R antagonist properties as con-T, was similarly investigated. The results demonstrated that apo-con-G is largely in a randomly dispersed conformation, whereas the Ca^{2+}-loaded and, especially, the Mg^{2+}-loaded forms of this peptide possessed a very distinct α-helical conformation. In addition, the Ca^{2+}- or Mg^{2+}-induced conformations of con-G are both amino- to carboxyl-terminal end-to-end α-helices. A superimposition of Ca^{2+}/con-T (12) and Mg^{2+}/con-G structures shows a large degree of similarity for the peptide backbone (Fig. 6). That both peptides with the same biological properties adopt a very similar structure again suggests that an α-helix may be the bioactive conformation for both con-G and con-T.

Properties of Con-G Mutants—A number of mutant peptides have been constructed to attempt to assess the importance of individual Gla residues in cation binding and cation-dependent properties of con-G. From the model of Fig. 7, it appears as though all Gla residues are involved in cation binding, a situation that contrasts to that of con-T, wherein Gla^4 does not appear to participate in metal ion coordination. The presence of the centrally located Gla^7 in con-G, a residue absent in con-T, appears to bestow somewhat different metal ion binding properties on this peptide. Under the conditions employed in our direct Mg^{2+} binding studies, wild-type con-G harbors two binding sites, whereas all of the Gla-derived mutants possess only a single site (Table II). Although it is not necessarily the case that all of these mutants bind Mg^{2+} in a manner similar to the parent peptide (they could behave as independent and nonrelated peptides in this regard), and this could be reflected in the intermediate values of the K_d values for the single site in the Gla^4Ala and Gla^{10}Ala mutants (Table II), the situation that Mg^{2+} binding of the variant peptides can be modeled solely by considerations of cation binding to wild-type con-G will be assumed to be true simply for purposes of this discussion. If it is the case, then, from Table II, it appears that Gla^{10} and Gla^{14} coordinate the tight Mg^{2+} site, whereas Gla^3, Gla^4, and Gla^7 appear to make up the weaker cation site. This conclusion is fortified by the NMR data of Table S1a–c, wherein the chemical shifts of the γCH protons of these Gla residues are significantly shifted in the presence of Mg^{2+}. The only uncertainty concerns Gla^4, which does not undergo a pronounced chemical shift of its γCH proton upon addition of Mg^{2+}. Thus, its significant effect on Mg^{2+} binding (Table II) may reside in a deleterious effect of its mutation on the conformation of the peptide at its amino-terminal region. Specifically, the first four αNH groups are not hydrogen bonded, and Gla^4 may be required for stabilization of the α-helix in this location by capping amino-terminal backbone amides. Thus, replacement of this residue by Ala might disrupt the α-helix or prevent its formation at the amino terminus of the peptide and in this way affect metal binding indirectly. Further studies with additional peptide variants are required to arrive at more firm conclusions regarding whether the role of Gla^4 in cation binding is direct or indirect.

Each of the Gla residues of con-G appears to be involved in the ability of this peptide to assume its full cation-dependent α-helical conformation (Table II). However, in each case, the C_{50} for Mg^{2+}, which characterizes the Mg^{2+} dependence of this conformational change, reflects the K_d for Mg^{2+} determined from direct binding studies. This shows that the tight and weak metal binding sites all contribute to the ability of con-G to assume the metal-dependent conformation and that both sets of binding sites, as enforced by the full complement of Gla residues, need to be occupied for this maximum alteration to occur.

Conclusions—This study has provided compelling structural evidence that further supports our original position that con-G exhibits no conformational preference in the absence of divalent metal ions. In addition, it has served to explain the effects of Ca^{2+} and Mg^{2+} binding on the peptide structure of con-G. The lack of sufficient con-G/Ca^{2+} NOE distance constraints to fully define side-chain orientations appears to be directly related to its lower metal ion affinity. In contrast, the tighter binding Mg^{2+} ions allowed a detailed structural analysis to be performed that was of a resolution sufficiently high to confidently predict metal binding sites. Thus, when comparing the effects of these two physiologically relevant metals, it is concluded that Mg^{2+}, and not Ca^{2+}, is likely the major contributor to the bioactive conformation of con-G.

[6] E. D. Rosen, personal communication.

REFERENCES

1. Olivera, B. M., Rivier, J., Clark, C., Ramilo, C. A., Corpuz, G. P., Abogadie, F. C., Mena, E. E., Woodward, S. R., Hillyard, D. R., and Cruz, L. J. (1990) *Science* **249,** 257–263
2. Myers, R. A., McIntosh, M., Imperial, J., Williams, R. W., Oas, T., Haack, J. A., Hernandez, J.-F., Rivier, J., Cruz, L. J., and Olivera, B. M. (1990) *J. Toxicol. Toxin Rev.* **9,** 179–202
3. McIntosh, J., Olivera, B. M., Cruz, L., and Gray, W. (1984) *J. Biol. Chem.* **259,** 14343–14346
4. Haack, J. A., Rivier, J., Parks, T. N., Mena, E. E., Cruz, L. J., and Olivera, B. M. (1990) *J. Biol. Chem.* **265,** 6025–6029
5. Skolnick, P., Boje, K., Miller, R., Pennington, M., and Maccecchini, M.-L. (1992) *J. Neurochem.* **59,** 1516–1521
6. Prorok, M., Warder, S. E., Blandl, T., and Castellino, F. J. (1996) *Biochemistry* **35,** 16528–16534
7. Rigby, A. C., Baleja, J. D., Furie, B. C., and Furie, B. (1997) *Biochemistry* **36,** 6906–6914
8. Zhou, L.-M., Szendrei, G. I., Fossom, L. H., Maccecchini, M.-L., Skolnick, P., and Otvos, L. (1996) *J. Neurochem.* **66,** 620–628
9. Skjaerbaek, N., Nielsen, K. J., Lewis, R. J., Alewood, P., and Craik, D. J. (1997) *J. Biol. Chem.* **272,** 2291–2299
10. Lin, C. H., Chen, C. S., Hsu, K. S., King, D. S., and Lyu, P. C. (1997) *FEBS Lett.* **407,** 243–248
11. Warder, S. E., Chen, Z. G., Zhu, Y., Prorok, M., Castellino, F. J., and Ni, F. (1997) *FEBS Lett.* **411,** 19–26
12. Warder, S. E., Prorok, M., Chen, Z., Li, L., Zhu, Y., Pedersen, L. G., Ni, F., and Castellino, F. J. (1998) *J. Biol. Chem.* **273,** 7512–7522
13. Colpitts, T. L., and Castellino, F. J. (1993) *Int. J. Pept. Protein Res.* **41,** 567–575
14. Piotto, M., Saudek, V., and Sklenar, V. (1992) *J. Biomol. NMR* **2,** 661–665
15. Lippens, G., Dhalluin, C., and Wieruszeski, J.-M. (1995) *J. Biomol. NMR* **5,** 327–331
16. Braunschweiler, L., and Ernst, R. R. (1983) *J. Magn. Reson.* **53,** 521–528
17. Davis, D. G., and Bax, A. (1985) *J. Am. Chem. Soc.* **107,** 2820–2821
18. Kadkhodaei, M., Hwang, T.-L., Tang, J., and Shaka, A. J. (1993) *J. Mag. Reson.* **A 105,** 104–107

19. Rance, M., Sorenson, O. W., Bodenhausen, G., Wagner, G., Ernst, R. R., and Wüthrich, K. (1983) *Biochem. Biophys. Res. Commun.* **117,** 479–495
20. Marion, D., and Wüthrich, K. (1983) *Biochem. Biophys. Res. Commun.* **113,** 967–974
21. Ni, F., Ripoll, D. R., and Purisima, E. O. (1992) *Biochemistry* **31,** 2545–2554
22. Kim, Y., and Prestegard, J. H. (1989) *J. Magn. Reson.* **84,** 9–13
23. Wüthrich, K. (1986) *NMR of Proteins and Nucleic Acids,* John Wiley & Sons, Inc., New York
24. Némethy, G., Gibson., K. D., Palmer, K. A., Yoon, C. N., Paterlini, G., Zagari, A., Rumsey, S., and Schereaga, H. A. (1992) *J. Phys. Chem.* **96,** 6472–6484
25. Ni, F., Konishi, Y., Bullock, L. D., Rivetna, M. N., and Scheraga, H. (1989) *Biochemistry* **28,** 3106–3119
26. Ni, F., Zhu, Y. i., and Scheraga, H. A. (1995) *J. Mol. Biol.* **252,** 656–671
27. Vásquez, M., and Scheraga, H. A. (1988) *J. Biomol. Struct. Dyn.* **5,** 757–784
28. Li, L., Darden, T. A., Freedman, S. J., Furie, B. C., Furie, B., Baleja, J. D., Smith, H., Hiskey, R. G., and Pedersen, L. G. (1997) *Biochemistry* **36,** 2132–2138
29. Pearlman, D. A., Case, D. A., Caldwell, J. W., Ross, W. S., Cheatham, T. E. I., Ferguson, D. M., Seibel, G. L., Singh, U. C., Weiner, P. K., and Kollman, P. A. (1995) *Amber*, Version 4.1, University of California, San Francisco
30. Essmann, U., Perera, L., Berkowitz, M. L., Darden, T., Lee, H., and Pedersen, L. G. (1995) *J. Chem. Phys.* **103,** 8577–8593
31. Chen, Y.-H., Yang, J. T., and Martinez, H. M. (1972) *Biochemistry* **11,** 4120–4131
32. Wishart, D. S., Sykes, B. D., and Richards, F. M. (1992) *Biochemistry* **31,** 1647–1651
33. Blandl, T., Zajicek, Y., and Castellino, F. J. (1997) *Biochem. J.* **328,** 777–783
34. Wiseman, T., Williston, S., Brandts, J. F., and Lin, L.-N. (1989) *Anal. Biochem.* **179,** 131–137
35. Mayer, M. L., Westbrook, G. L., and Guthrie, P. B. (1984) *Nature* **309,** 261–263